Journal of the Meteorological Society of Japan, Vol. 82, No. 2, pp. 745–759, 2004

Effects of Large-scale Orography on the Coupled Atmosphere-Ocean System in the Tropical Indian and Pacific Oceans in Boreal Summer

Manabu ABE

Doctoral program in Geoscience, University of Tsukuba, Tsukuba, Japan

Tetsuzo YASUNARI[1]

Institute of Geoscience, University of Tsukuba, Tsukuba, Japan

and

Akio KITOH

Meteorological Research Institute, Tsukuba, Japan

(Manuscript received 11 December 2002, in revised form 24 December 2003)

Abstract

We investigated the effects of large-scale orography on the tropical coupled atmosphere-ocean system over the Indian and Pacific Oceans in northern summer, using the Meteorological Research Institute coupled atmosphere-ocean General Circulation Model (GCM). Six different experiments were conducted with mountain heights of 100%, 80%, 60%, 40%, 20%, and 0% of the standard mountain height. The results show that a pool of warm sea surface temperatures (SSTs) appears in the western Pacific as orography increases, although SST in the tropical Pacific decreases as a whole. In addition, easterly winds at low levels over the equatorial Pacific strengthen as mountains rise. The enhanced easterlies alter surface heat flux and ocean dynamics, changing the water temperature field in the upper Pacific Ocean. Water temperatures between the surface and 300 m in the western Pacific increase as upwelling is suppressed and the thermocline deepens. Water temperatures in the eastern Pacific decrease and the thermocline rises. Therefore, the east-west gradient of water temperature in the Pacific is enhanced for cases with mountain heights of 80% and 100% of the standard mountain height. In the equatorial Indian Ocean, the east-west gradient of ocean heat content weakens as mountain heights increase, in connection with the evolution of the Asian summer monsoon. An increase in diabatic heating over South Asia as mountain heights increase causes sea level pressure (SLP) to decline over the Indian Ocean, and enhances upper atmospheric divergence over the eastern hemisphere. Consequently, the east-west circulation over the Indian and Pacific Oceans strengthens as mountains become taller. The east-west circulation may also be enhanced by changes in convective activity associated with SST changes. The coupled general circu-

Corresponding author and present affiliation: Manabu Abe, Graduate school of Environmental studies, Nagoya University, Nagoya, Japan. Lab: Hydrospheric Atmospheric Research Center, Nagoya University, Furo-cho, Chikusa-ku, Nagoya, 464-8601, Japan.
E-mail: mabe@hyarc.nagoya-u.ac.jp

1 Present affiliation: Hydrospheric Atmospheric Research Center, Nagoya University, Nagoya, Japan.

lation model (GCM) results show that uplift of large-scale orography, particularly the Tibetan Plateau, significantly affects the tropical atmospheric and oceanic climate, by changing the east-west circulation and altering the evolution of the Asian summer monsoon.

1. Introduction

Sea surface temperatures (SSTs) in the tropical Pacific are characterized by warm temperatures in the western Pacific, and cold temperatures in the eastern Pacific. The heat source associated with the western Pacific warm pool is a critical element of the global climate (Palmer and Mansfield 1984). A variety of influences affect the temperature distribution. Advection induced by surface wind stresses strongly influences the SST pattern. Westward currents in the tropical Pacific transport cold water that upwells along the American coast. The SST patterns also reflect subsurface thermal gradients. The decrease in SSTs from west to east along the Equator is associated with a shoaling of the isotherms: the thermocline in the western equatorial Pacific is at about 150 m depth; the thermocline in the eastern equatorial Pacific is shallower. Atmospheric convection over the tropical ocean is strongly associated with the SST pattern. Convection frequently occurs over the warm SSTs. Such convection alters both the atmospheric circulation and the ocean surface.

The El Niño and Southern Oscillation (ENSO) phenomenon is a large-scale coupled atmosphere-ocean system in the tropics, with multi-year variability that affects the global atmospheric circulation (e.g., Yasunari 1987). A positive SST anomaly occurs in the eastern Pacific during El Niño. ENSO events depend on abnormal conditions in the western Pacific, such as atmospheric westerly wind bursts and positive anomalies of ocean heat content. Wyrtki (1975) suggested that a thick and warm oceanic mixed layer in the western equatorial Pacific is an important factor controlling the start of El Niño events in the eastern Pacific. In addition, through the east-west circulation the Asian summer monsoon may actively control the interannual variability of the coupled atmosphere-ocean system in the tropical Pacific (Yasunari 1990). This relationship between the Asian summer monsoon, and the tropical Pacific, may be significant for the formation of the tropical climate. It is therefore essential to investigate the controls on the tropical summer climate over the Pacific and the Indian Oceans as a coupled atmosphere-ocean system that includes the Asian summer monsoon, which is enhanced by mountain uplift (Abe et al. 2003).

Large-scale orography influences formation of the global climate through dynamical, and thermodynamical effects (Kutzbach et al. 1993). The role of large-scale orography on climate has been investigated using general circulation models (GCMs) in many previous studies (e.g., Hahn and Manabe 1975; Kutzbach et al. 1989; Kutzbach et al. 1993). Atmospheric GCMs (AGCMs) that included a prescribed observed SST have been used in previous studies to examine the effects of changing orography on the Asian monsoon (e.g., Hahn and Manabe 1975; Kutzbach et al. 1989; Liu and Yin 2002). Kitoh (2002) used a coupled atmosphere-ocean GCM (CGCM) to investigate the effects of orography on the annual mean surface global climate, and showed that SST distributions, atmospheric and oceanic circulations, and land surface climate all changed as orography changed. To understand fully the effects of orography on climate, changes in oceanic circulation must be considered. Few studies have examined the effects of large-scale orography on climate in the Pacific and Indian Oceans, and most previous studies used AGCM, not CGCM.

Abe et al. (2003) used the Meteorological Research Institute (MRI) CGCM-I to study the influence of mountain uplift on the evolution of the Asian summer monsoon. Precipitation associated with the South Asian summer monsoon increased as mountain increased, and monsoon circulations, such as the low-level southwesterly monsoon, were also enhanced. Atmospheric changes, such as the altered Asian summer monsoon, can influence the tropical ocean through air-sea interactions.

In this paper, the effects of large-scale orography on the mean state of a coupled atmosphere-ocean system in the tropical Indian and Pacific Oceans in boreal summer, were investigated using varying mountain heights, using the same experimental data as used in Abe et al. (2003).

2. Model and experimental design

This study uses the coupled global atmosphere-ocean GCM developed at the MRI (MRI CGCM I, Tokioka et al. 1995). The atmospheric model has a horizontal resolution of 5° longitude by 4° latitude and 15 vertical levels. The top of the atmosphere is at 1 hPa. Shortwave radiation is parameterized as in Lacis and Hansen (1974). Rayleigh scattering and absorption by ozone, water vapor and carbon dioxide are also calculated. Longwave radiation calculations are based on the multiparameter random model of Shibata and Aoki (1989). The model uses a version of the Arakawa-Schubert penetrative cumulus convection parameterization (Tokioka et al. 1988). Orographic gravity-wave drag calculations follow Palmer et al. (1986). The land surface has four levels, with a bottom at 10 m; ground temperature, soil moisture, and frozen soil moisture are prognostic variables at each level. Kitoh et al. (1995) described the performance of the AGCM.

The ocean general circulation model (OGCM) was also developed at MRI (Nagai et al. 1992). The OGCM has nonuniform meridional resolution ranging from 0.5° to 2.0°, with a finer grid in the tropics, and a fixed zonal resolution of 2.5°. There are 21 vertical levels in the OGCM, which includes realistic bottom topography. The Mellor-Yamada level-2 turbulence closure scheme simulates the oceanic mixed layer. The original model predicts sea ice concentration and thickness, but for this study fixed monthly sea ice conditions (concentration and thickness), based on observations were prescribed for all runs.

Six runs (M, M8, M6, M4, M2, and M0) were integrated for 50 years, separately. Run M was the control with standard orography. Runs M8, M6, M4, M2 and M0 included 80%, 60%, 40%, 20% and 0% of the global orography in M, respectively. All runs started from the same initial condition with the standard orography as in M. In runs M0, M2, M4, M6, and M8, the orography slowly decreased by 10% of the present mountain height per month, to avoid a termination of integration due to rapid change of boundary condition. This slow change in the boundary allowed continued time integration. When the orography in each run reached the desired percentage of the standard height, the integration continued with a fixed, reduced mountain height. Flux adjustments for surface energy and water fluxes were operated to simulate realistic SSTs, and sea surface salinity fields in the control run (M). Because true climatological states of SST and surface salinity in the other runs are unknown, flux adjustments in all runs used the adjustment data used in M. Figure 1 shows time series of annual mean SST and water temperature at 350 m depth in the western (140°E–160°E, 6°S–6°N) and eastern (100°W–80°W, 6°S–6°N) Pacific in M and M0. SSTs are greater in the western Pacific than in the eastern Pacific, and SSTs in both the western and eastern Pacific are cooler in M than M0. Note that SSTs have adjusted within 5 years in M0. Water temperature at 350 m seems to equilibrate within about 10 years in M0, although the temperature in M and M0 decreases at a rate of about 0.2°C per 10 years. The deeper ocean does not reach equilibrium, because the deeper ocean has a much longer time scale of variability. The focus in this paper is on circulation changes in the atmosphere and in the ocean above 300 m. Seasonal mean data for June–August, averaged for the last 30 years of integration, are used hereafter for analysis. Figure 2 shows the seasonal mean precipitation and SSTs during June-August in M. Simulated large-scale precipitation coincides with climatology based on observations. The Intertropical Convergence Zone (ITCZ) and the South Pacific Convergence Zone (SPCZ) are over the Pacific. Further, there is larger precipitation in the western Pacific. The SST pattern is reasonably reproduced because of flux adjustments. A cold tongue simulated in the eastern Pacific, and a warm pool in the western Pacific, are similar to observations.

Kitoh et al. (1999) investigated the climatological mean and the interannual variability of the Asian monsoon, and the atmosphere-ocean system over the Pacific in this CGCM and found that features in this CGCM were close to observations. Furthermore, the interdecadal variability in the Pacific in the CGCM is realistic (Yukimoto et al. 1996).

3. The tropical Pacific and Indian Ocean

This section describes changes in ocean temperatures in the equatorial Pacific and Indian Oceans. Figure 3 shows seasonal mean SSTs

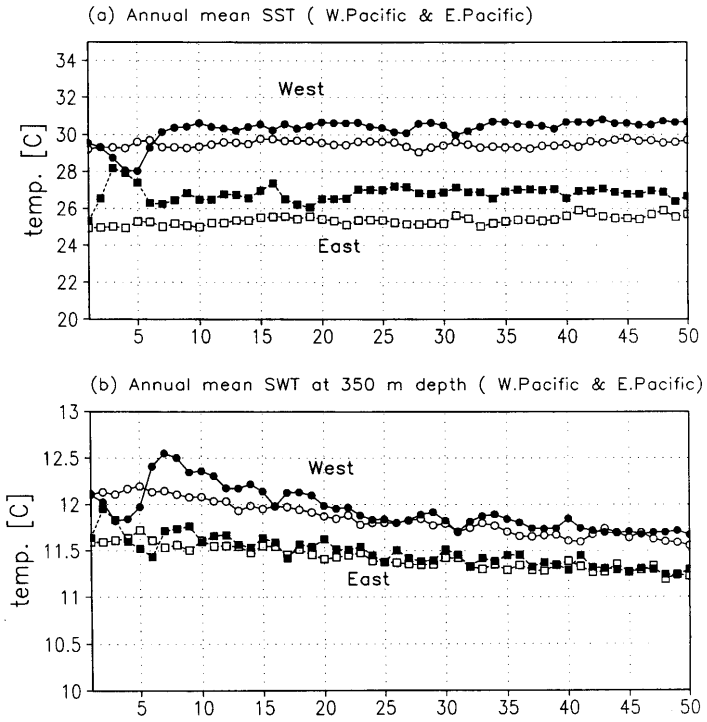

Fig. 1. Time series of (a) annual mean SST and (b) sea water temperature at 350 m depth in the western Pacific (140°E–160°E, 6°S–6°N) and the eastern Pacific (100°W–80°W, 6°S–6°N). Open (closed) circle shows value in the western Pacific in M (M0), and Open (closed) square shows value in the eastern Pacific in M (M0). Units are °C.

during June–August in all runs. A remarkable feature in these figures is the cooler SSTs in the tropical Pacific with mountain uplift. SSTs exceed 31°C in the central Pacific (150°E–180°) in experiments M0 to M6, but not in M8 or M. Ocean cooling as mountains build is caused by several effects; such as increased evaporation and enhanced oceanic upwelling, forced by stronger surface winds enhanced by mountain uplift, and decreased shortwave insolation into the ocean, associated with increased cloud and convection (Abe et al. 2003). Cooler SSTs in the central-eastern Pacific at 10°N–30°N are associated with a subtropical anticyclone in the North Pacific that strengthens as mountains get taller because of the increased heat contrast between land and ocean in mid-latitudes. Kitoh (2002) showed SST decreases in the same region as a result of changes in surface fluxes of latent heat and shortwave radiation. Figure 4 shows seasonal mean surface latent heat flux for June–August in all runs. Latent heat flux in the subtropical central north Pacific (180°–140°W, 10°N–30°N) is less than 140 W m^{-2} in M0. As mountains grow taller, the enhanced subtropical anticyclone in the North Pacific, due to mountain uplift, forces stronger winds that increase the latent heat flux. Latent heat flux exceeds 140 W m^{-2} in the subtropical central north Pacific in M6, M8, and M. Figure 5 shows seasonal mean surface shortwave radiation flux for June–August for all runs. Positive values indicate downward fluxes. The flux in the region (150°W–120°W, 15°N–30°N) decreases as mountains build because of increased stratus clouds (not shown). Such changes in summer cool the SSTs over the eastern Pacific at 10°N–30°N, as noted in Kitoh (2002). However, in the western Pacific at 10°N–30°N, no remarkable SST change occurs with mountain uplift, except a general decrease in SSTs. Figure 6 shows the SST differences from the SST in the tropical western Pacific (135°E, 2°N) in each run to facilitate detecting

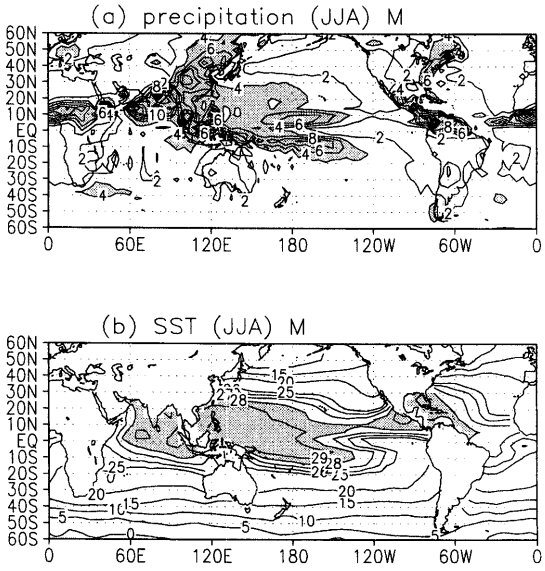

Fig. 2. (a) Seasonal mean precipitation during June–August in M (control run). Unit is mm day^{-1}. Contour interval is 2 mm day^{-1}. Precipitation above 4 mm day^{-1} are shaded. (b) Seasonal mean SST during June–August in M. Unit is °C. Contour interval is 1°C. SST above 28°C are shaded.

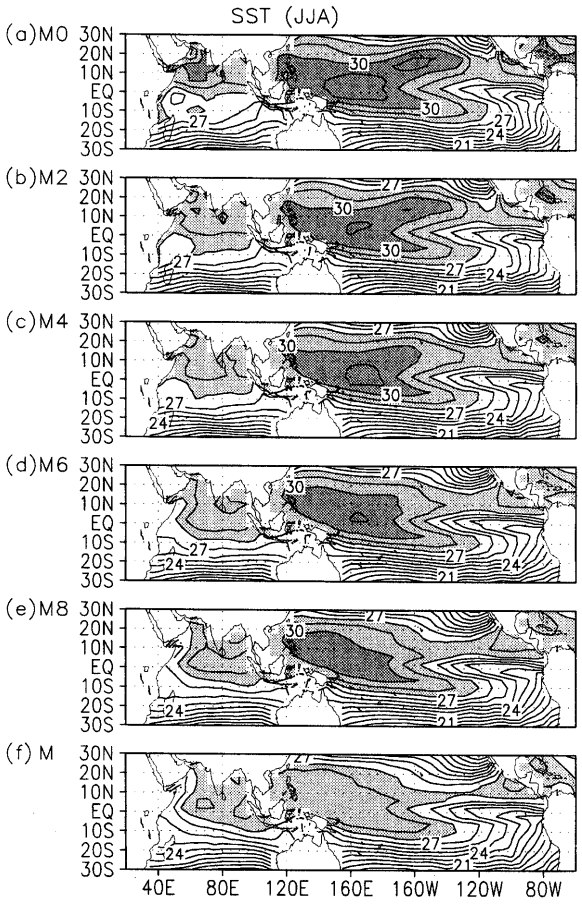

Fig. 3. Seasonal mean SSTs during June–August in all runs. Units are °C. Contour interval is 1°C. Dark (light) shaded area indicates SST above 30°C (28°C).

changes in SSTs in the western Pacific, relative to other tropical oceans. Positive values extend northeastward from the central equatorial Pacific in M0. This positive value disappears with mountain uplift, as mentioned above. In the western Pacific, a positive value that extends from the Equator to 10°N in M0 expands north to 20°N in M6, M8, and M. An enhanced northwestward surface current, which is forced by amplified zonal wind velocities in the western Pacific as the mountains grow, contributes to the northward spread of the warmer water. Consequently, the zonal SST gradient near 10°N–30°N in the Pacific increases as mountains grow, and the warm western Pacific is recognizable in M.

Figure 7 shows the longitude-depth distributions of seasonal mean sea water temperature (SWT), and the ocean circulations between the surface and 300 m depth during June–August, averaged for 15°N–25°N in M0, and the differences between M8 and M0, and M and M0. Warm water (> 30°C) occurs in the eastern Pacific (Fig. 7a). The thermocline is not obvious in Fig. 7. Upwelling induced by northeasterly winds occurs in the eastern Pacific, and downwelling between the surface and about 100 m occurs in the western Pacific. In M8 and M, SWT in the central and eastern Pacific between the surface and about 120 m, decreases because of the enhanced subtropical anticyclone over the Pacific in summer. Cool water is transported from the north, and latent heat flux increases due to stronger winds. An increase in SWT between about 100 m and 300 m in the Pacific appears in M8 and M, with a core at about 240 m in the central Pacific. This warming is likely linked to enhanced downwelling in the central Pacific, where the convergence of the subsurface current increases

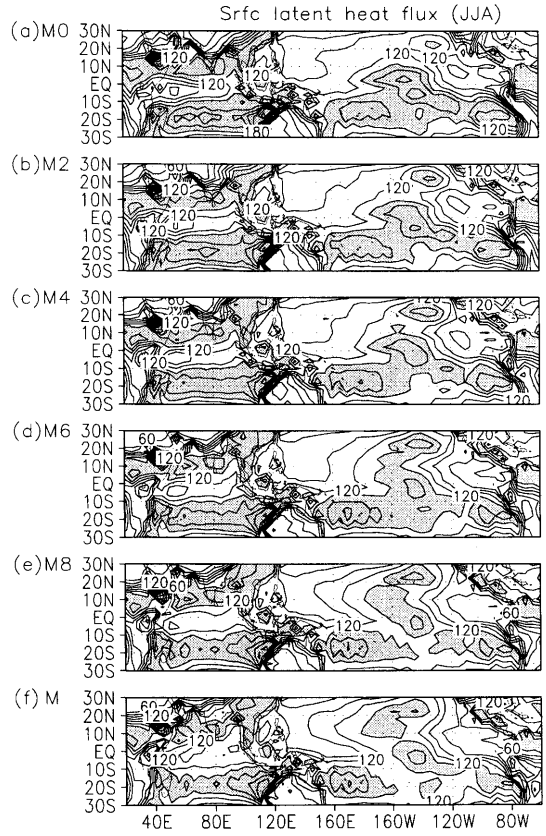

Fig. 4. Seasonal mean surface latent heat flux for June–August in all runs. Units are W m^{-2}, and contour interval is 20 W m^{-2}. Shaded area indicates value above 140 W m^{-2}.

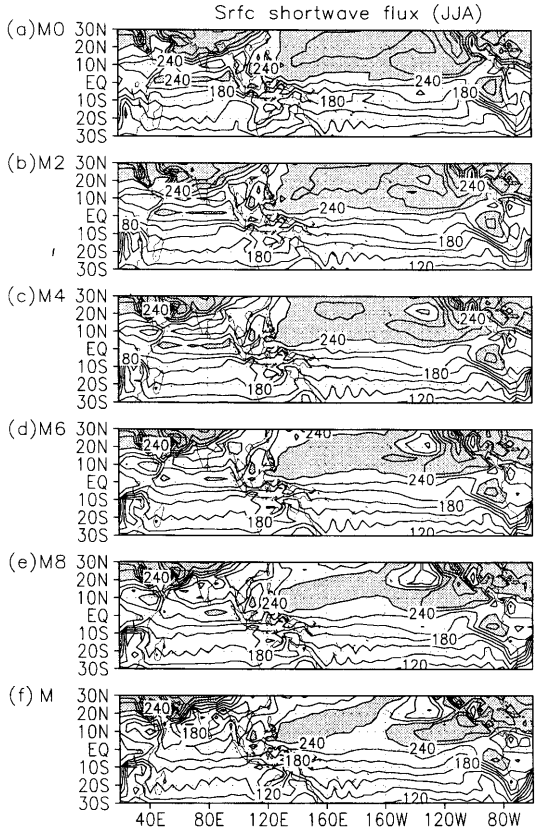

Fig. 5. Seasonal mean surface shortwave radiation flux for June–August in all runs. Units are W m^{-2}, and contour interval is 20 W m^{-2}. Values above 240 W m^{-2} are shaded.

because of the southwestward subsurface current, that is enhanced by the subtropical anticyclone, and the enhanced northward current near the Equator related to Ekman drift. In the western Pacific, in contrast, downwelling between the surface and 100 m is suppressed, and upwelling below 100 m strengthens in M8 and M. Changes in the western Pacific are related to enhanced easterlies. In the Indian Ocean, SSTs in M0 are warmer in the Northern Hemisphere, particularly in the Arabian Sea (Fig. 3a). As mountains grow, SSTs in the Arabian Sea and the Bay of Bengal decrease, and SSTs in the equatorial Indian Ocean increase in association with changes in the Asian summer monsoon. Enhanced low-level atmospheric southwesterlies near the Equator in the North Indian Ocean, strengthen the southward sea surface current and weaker atmospheric southeasterlies near the Equator, between 60°E–100°E in the Southern Hemisphere, weaken the southward sea surface current there. Thus, the flow of warm water converges in the equatorial Indian Ocean, and upwelling at the Equator is suppressed. Whereas SSTs in the eastern equatorial Indian Ocean increase, those in the western Indian Ocean decrease because of a stronger Somali Jet with mountains uplift. The SSTs in the Arabian Sea and the Bay of Bengal, decrease as mountains grow because solar insolation into the ocean is suppressed by clouds (Fig. 5) (Abe et al. 2003). The present SST distribution in the Indian Ocean is strongly governed by the Asian summer monsoon circulation, and paleo-climatological change of SSTs in the tropical Indian ocean

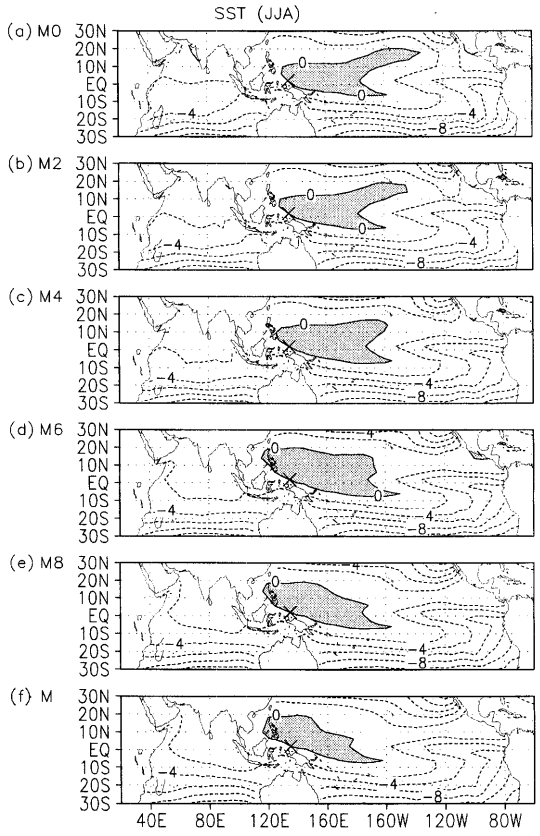

Fig. 6. Seasonal mean distributions of SST differences from SST in the tropical western Pacific (135°E, 2°N) for June–August in each run. Units are °C, and contour interval is 2°C. Positive values are shaded. An cross is marked at (135°E, 2°N).

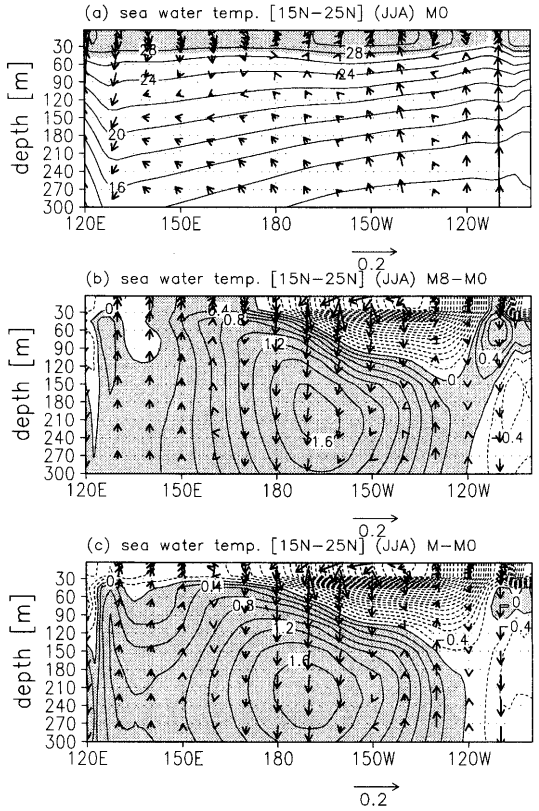

Fig. 7. (a) Longitude-depth cross section of seasonal mean sea water temperature, and the ocean circulation between the surface and 300 m depth during June–August, averaged for 15°N–25°N in M0. (b) (c) The differences between M8 and M0, and M and M0. Contour shows sea water temperature, and its units are °C. Vector indicates the ocean circulation, but that is drawn as the vertical velocity is 1×10^5 times the simulated value. Units of ocean circulation are m s^{-1}.

may be closely linked to the evolution of the Asian monsoon (e.g., Abe et al. 2003).

An east-west temperature gradient in the equatorial Pacific clearly exists in all runs. Figure 8 shows SST differences between the western Pacific (115°E–140°E, 2°S–2°N) and the eastern Pacific (95°W–85°W, 2°S–2°N), and sea level pressure (SLP) differences between the western Pacific (115°E–125°E, 10°S–10°N) and the eastern Pacific (105°W–95°W, 10°S–10°N). The ordinate indicates the amount of mountain uplift and the abscissa indicates SST or SLP. The SST gradient in the equatorial Pacific increases from east to west with mountain uplift; the largest increase occurs from M6 to M8. The SLP gradient between the eastern and western Pacific gradually increases (Fig. 8b). An abrupt increase in SLP gradient from M6 to M8 does not occur. Figure 9a shows a longitude-depth distribution of seasonal mean SWT and ocean circulation between the surface and 300 m depth during June–August in M0, averaged for 10°S–10°N. The deepest thermocline in M0 is about 150 m in the central Pacific, about 120 m in the western Pacific, and about 60 m in the eastern Pacific. Weaker upwelling in M0 appears near the surface in most of the Pacific and Indian Ocean, and weak downwelling occurs at the surface in the western Pacific. Be-

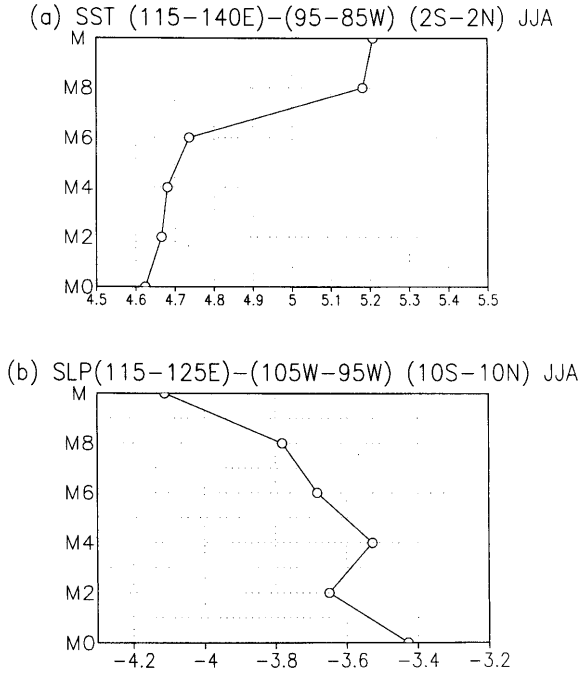

Fig. 8. (a) SST differences between the western Pacific (115°E–140°E, 2°S–2°N) and the eastern Pacific (95°W–85°W, 2°S–2°N) for June–August. (b) SLP differences between the western Pacific (115°E–125°E, 10°S–10°N) and the eastern Pacific (105°W–95°W, 10°S–10°N) for June–August. The ordinate indicates the amount of mountain uplift, and the abscissa indicates SST in (a), whose unit is °C, and SLP in (b), whose unit is hPa.

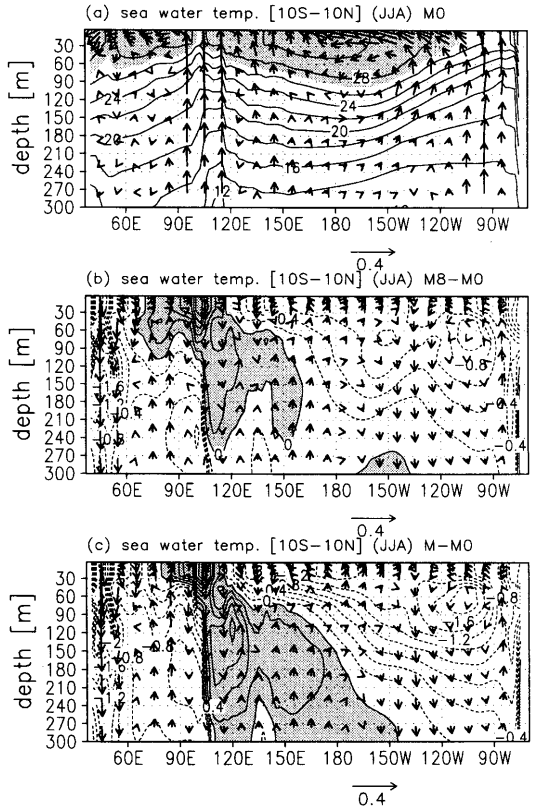

Fig. 9. (a) Longitude-depth cross section of seasonal mean sea water temperature and the ocean circulation between the surface and 300 m depth during June–August in M0, averaged for 10°S–10°N. (b) (c) Longitude-depth cross section of differences in seasonal mean sea water temperature and the ocean circulation, averaged for 10°S–10°N, between M8 and M0, and M and M0. Contour shows sea water temperature, and its units are °C. Vector indicates ocean circulation, but that is drawn as the vertical velocity is 1×10^5 times the simulated value. Units of ocean circulation are m s^{-1}.

cause the upwelling in the eastern Pacific occurs over deeper ocean, cool abyssal water is transported to the upper ocean. Thus, the thermocline in the eastern Pacific is particularly shallow even in M0, and a zonal gradient of oceanic heat content exists along the equatorial Pacific in M0. Figures 9b and 9c show longitude-depth distributions of differences in seasonal mean SWT and ocean circulation during June–August along the Equator (10°S–10°N) between M8 and M0, and M and M0, respectively. In M0 to M6, an overall decrease in SWT in the Pacific occurs, particularly at about 60 m in the eastern Pacific (not shown); the rate of decrease is smaller in the western Pacific than in the eastern Pacific. In M8 and M (Figs. 9b and 9c), SWT in the western Pacific increases from values in M0, and SWT in the eastern Pacific decreases further. The SWT increases particularly between 60 and 270 m in M and expands eastward to 180°. Upwelling in the western Pacific is suppressed by increased transport of surface water from the east by stronger surface zonal winds, and upwelling from the deeper ocean near the eastern Pacific coast strengthens. Therefore, the ocean

heat content increases (decreases), and the thermocline deepens (shoals) in the western (eastern) Pacific. Thus, La Niña-like conditions are enhanced in the tropical Pacific as mountains grow.

However, the easterlies over the western Pacific in the later stages of mountain uplift become stronger than those over the eastern Pacific. Because the subtropical high strengthens with enhanced topography, the southwestward ocean surface current also intensifies with mountain growth. Local changes in ocean circulation in the tropical Pacific, such as downwelling in the central Pacific, appear as mountains grow. The most important point to emphasize in this study is that the wide east-west gradient of ocean heat content in the tropical Pacific increases, due to changes in the atmospheric circulation as mountains grow. The thermocline is shallower in the eastern Indian Ocean than in the western Indian Ocean in M0. Comparisons of M8 and M with M0 show that subsurface upwelling in the eastern Indian Ocean weakens with mountain uplift. In contrast, upwelling in the western Indian Ocean strengthens, because surface atmospheric cross-equatorial southerlies strengthen. In addition, westward oceanic surface flow weakens, associated with the stronger atmospheric westerlies, as depicted by an eastward difference, in the surface ocean flow from M0 to M8 and M in Figs. 9b and 9c. Accordingly, SWT above 60 m increases in the eastern Indian Ocean and decreases in the western Indian Ocean. Thus, the east-west gradient of ocean heat contents in the equatorial Indian Ocean decreases in M. Enhancement of surface wind in the tropics as mountains rise, increases the zonal gradient of ocean heat contents in the tropical ocean, and also increases the latent heat. The next section describes atmospheric circulation changes in the tropical coupled atmosphere-ocean system.

4. Atmospheric circulation in the tropics

Large-scale orography enhances the Asian summer monsoon; a stronger southwesterly monsoon enhances the inland penetration of convection (Abe et al. 2003). Previous observational studies have linked variability in the Asian summer monsoon to the atmospheric circulation over the tropical Pacific Ocean (e.g., Yasunari 1990, 1992). This study shows that the summer tropical atmospheric circulation is also affected by mountain height. The atmospheric changes linked to large-scale orography can also change the ocean circulation in the CGCM used in this study, which subsequently influences atmospheric circulation through air-sea interactions.

This section describes changes in the tropical atmospheric circulation in boreal summer (JJA). These results are attributed directly to changes in orography, and indirectly to SST changes forced by atmospheric changes. Figure 10 shows the mean zonal wind at 850 hPa for June–August in all runs. Easterly winds cover the entire equatorial Pacific Ocean; maximum speeds are near 140°W in all runs. Easterlies over the equatorial Pacific strengthen as

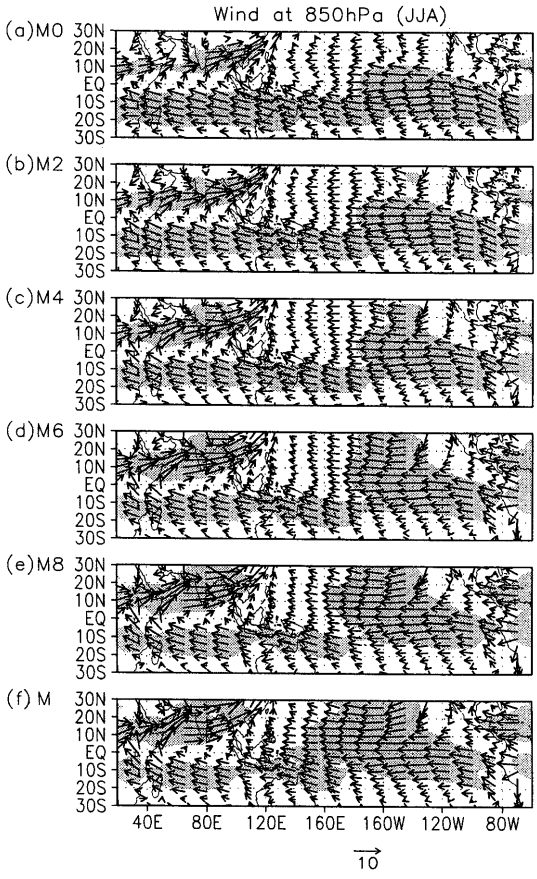

Fig. 10. Seasonal mean wind at 850 hPa during June–August in all runs. Units are m s^{-1}. Shaded area indicates zonal wind velocity is above 5 m s^{-1}.

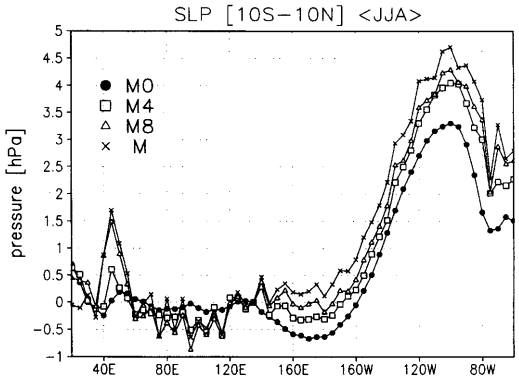

Fig. 11. Longitudinal distribution of seasonal mean SLP differences from SLP at 135°E for June–August in M0 (closed circle), M4 (open square), M8 (open triangle), and M (cross), averaged between 10°S and 10°N. Unit of pressure is hPa.

mountains rise, particularly over the western Pacific (west of the dateline) in M. In addition, easterlies strengthen near 10°N–30°N over the central and eastern Pacific, in association with the stronger subtropical anticyclone present in runs with taller mountains. Stronger easterlies promote surface evaporation, causing cooler SSTs, as described in the previous section.

Figure 11 shows the longitudinal distribution of seasonal mean sea level pressure (SLP) during June–August in M0, M4, M8, and M, averaged between 10°S and 10°N. SLP values are plotted as the difference from SLP at 135°E to simplify comparisons along the Equator. The SLP difference in the west central Pacific (west of 160°W) is negative in M0, consistent with the warm SSTs (> 30°C) in run M0. In the Indian Ocean, smaller negative values in M0 occur. SLP differences over the central and eastern Pacific increase to positive values in run M. The positive SLP difference in M over the west-central Pacific is consistent with the reduction of local warm SSTs relative to M0. The SLP difference over the eastern Indian Ocean decreases as mountains rise, because SSTs in the equatorial Indian Ocean increase, in association with the evolution of the Asian summer monsoon. Furthermore, a west-east gradient of SLP over the equatorial Indian Ocean appears in runs with higher mountains. The broad pressure gradient from the Indian Ocean to the Pacific Ocean increases as a result.

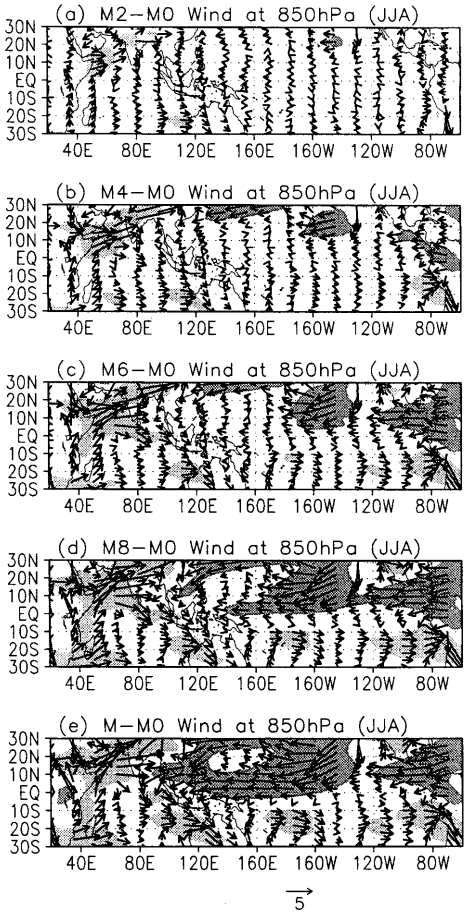

Fig. 12. Differences in seasonal mean wind at 850 hPa between M0 and the other runs for June–August. Units are m s^{-1}. Dark (light) shaded area indicates the difference in zonal wind velocity is above 2 m s^{-1} (below −2 m s^{-1}).

Figure 12 shows differences in wind at 850 hPa between M0 and the other runs. The enhancement in easterlies from 10°N–30°N, over the central and eastern Pacific noted above is obvious. The southwesterly Asian summer monsoon strengthens in runs with higher mountains. Differences in easterlies over the western Pacific are associated with changes in the broad zonal SLP gradient in runs with higher mountains. The 850 hPa wind difference is small for runs M2, M4, and M6, but becomes quite large for M8 and M. Furthermore, in M, low-level convergence is enhanced over the maritime continent between the Pacific and the Indian Ocean (Fig. 12e).

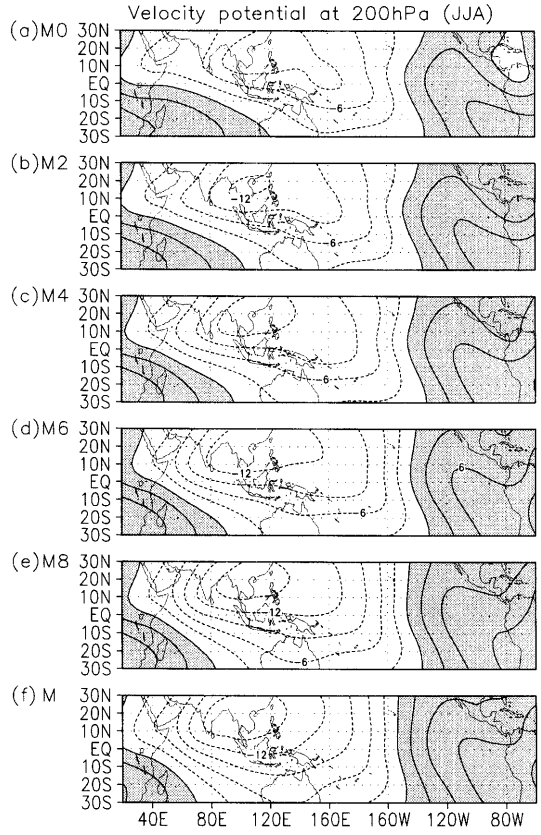

Fig. 13. Seasonal mean velocity potential at 200 hPa during June–August in all runs. Units are 1×10^6 m^2 s^{-1}. Positive (negative) values, which are shaded (not shaded), indicate convergence (divergence).

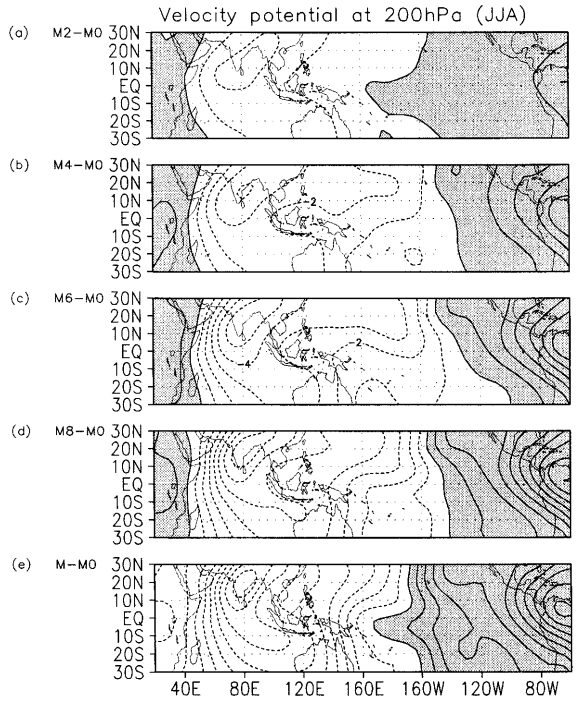

Fig. 14. Differences in seasonal mean velocity potential at 200 hPa, between M0 and the other runs for June–August. Units are 1×10^6 m^2 s^{-1}. Positive values are shaded.

Figure 13 shows mean velocity potential at 200 hPa for June–August in all runs. Divergence (negative values) is centered over Indochina and the South China Sea in M0, and convergence is centered over the south Atlantic Ocean. Weak divergence in M0 also occurs in the equatorial Pacific at about 160°E. The divergence center over Southeast Asia grows, and expands westward in the runs with higher mountains, as velocity potential increases over the Western Hemisphere. Figure 14 shows differences in seasonal mean velocity potential at 200 hPa between M0 and the other runs. Negative velocity potential values centered over India decrease as mountains rise: divergence over South Asia strengthens. At the same time, the convergence of velocity potential centered over northern South America increases as mountains rise, and velocity potential divergence at 10°N–30°N over the western Pacific also strengthens, particularly from M4 to M8. The changes in velocity potential should be linked to precipitation changes. Figure 15 shows the difference in seasonal mean precipitation for June–August between M and M0. Enhancement of convective activity in South Asia with higher mountains is reflected in stronger divergence fields in the Eastern Hemisphere, as shown in Fig. 13f. Similarly, the precipitation decrease found over northern South America with mountain uplift is consistent with enhanced convergence at 200 hPa. The east-west circulation (the Walker circulation) between tropical Asia and the tropical Pacific strengthens with mountain uplift, because of stronger diabatic heating associated with the increased convection over South Asia. Because higher mountains enhance the subtropical high, the east-west circulation between Asia and the eastern Pacific also strengthens in low latitudes. Precipitation decreases near 10°N–

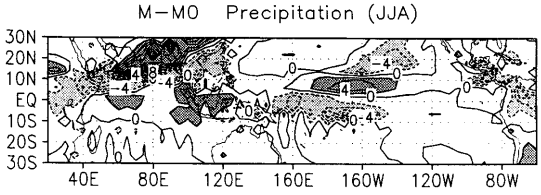

Fig. 15. Differences of seasonal mean precipitation for June–August between M and M0. Units are mm day^{-1}. Dark (light) shaded area indicates value above 2 mm day^{-1} (below −2 mm day^{-1}).

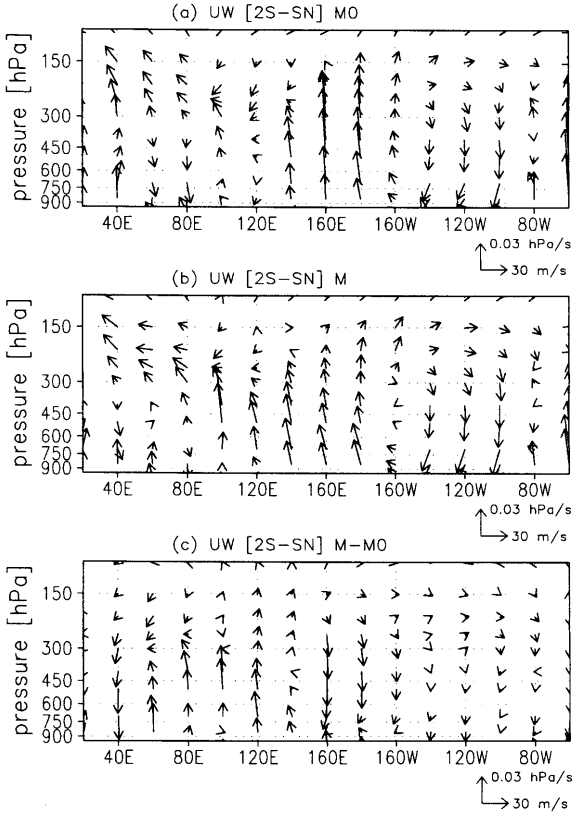

Fig. 16. Longitude-pressure cross sections of the zonal and vertical wind along the Equator (2°S–2°N) in (a) M0 and (b) M. The difference between M and M0 is also plotted in (c). Units of vertical velocity are hPa s^{-1}, and that of zonal velocity are m s^{-1}.

30°N over the central and eastern Pacific, because of cooler SSTs associated with mountain uplift. Near (160°E–160°W, 10°N), enhanced low-level convergence forces increased precipitation as mountains grow.

Figure 16 shows longitude-pressure (height) cross sections of mean zonal and vertical winds during June–August along the Equator in M0 and M, averaged between 2°S and 2°N. The difference between M0 and M is also plotted. Ascending motion from the surface to the upper troposphere clearly exists in M0 over the Pacific between 150°E and 180°; there is descending motion over the eastern Pacific. Further, weak ascent occurs over the western Indian Ocean in M0, and descent occurs over the central and eastern Indian Ocean. Downward motion is present in Fig. 16c between 150°E and 180°, where stronger ascent associated with convective activity is noted in M0. The suppressed ascent may be linked to the cooler SSTs caused by enhanced easterlies. The precipitation decrease west of 180°, as shown in Fig. 15, is consistent with suppressed ascent. In contrast, an upward difference vector exists west of 150°E, a region including the western Pacific and the eastern Indian Ocean, which indicates stronger ascent in M. The stronger ascent corresponds to amplified convective activity west of 150°E over the western Pacific Ocean, over the maritime continent, and over the eastern Indian Ocean. Changes in vertical circulation and convective activity are most remarkable in comparisons with M8 and M, rather than in comparisons of cases with smaller mountains.

The runs with high mountains have a strong east-west (Walker) circulation between eastern Asia and the central/eastern Pacific Ocean, which increases the heat contained in the upper ocean of the western Pacific, as noted in the previous section. Therefore, the zonal SWT gradient increases in the equatorial Pacific, particularly for M8 and M, as compared to cases with smaller mountains. The SST changes, in turn, are likely to suppress convection in the central Pacific (around the Dateline). Thus, ascent over the central Pacific may weaken, as in Fig. 16c. However, convective activity west of the central Pacific is enhanced by relatively warmer SSTs associated with the enhanced east-west circulation. Over the equatorial Indian Ocean, SSTs increase and the SWT east-west gradient decreases as the Asian

summer monsoon, evolves in runs with higher mountains. At the same time, convection and diabatic heating increases from the eastern Indian Ocean to the maritime continent. Such changes are consistent with enhancement of the east-west circulation along the Equator.

Thus, feedback exists between the atmosphere and the ocean. Changes in the atmosphere circulation, forced by mountain uplift affect the ocean circulation, which in turn is likely to affect atmospheric circulation systems, including the Asian summer monsoon and the Walker circulation.

5. Concluding remarks

A coupled atmosphere-ocean GCM (MRI CGCM-I) was used to study the effects of large-scale orography on the coupled tropical atmosphere-ocean system over the Indian and Pacific Oceans. The mountain heights in the model differed over six runs by 100% (control run), 80%, 60%, 40%, 20% and 0% of present standard mountain height. The land-sea distribution was the same for all runs.

SSTs in the tropical Pacific decrease as mountains rise, because of increased evaporation, decreased solar insolation at the surface because of increased cloudiness, and changes in ocean dynamics (e.g., upwelling) caused by changes in the atmospheric circulation. A large change in SST occurs at 10°N–30°N in the central-eastern Pacific in association with accelerated atmospheric easterlies. Furthermore, the decrease in solar insolation at the sea surface due to cloud effects, contributes to cooler SSTs over the eastern Pacific, as Kitoh (2002) noted. Warmer SSTs expand northward in the western Pacific in association with the accelerated atmospheric easterlies over the equatorial western Pacific, which induce a stronger poleward sea surface current. Low-level atmospheric circulation changes, that are associated with the evolution of the Asian summer monsoon, increase SSTs and therefore precipitation in the equatorial eastern Indian Ocean. A decrease in solar insolation cools SSTs over the Arabian Sea and the Bay of Bengal. These results strongly suggest that the SST distribution in the present Indian Ocean in summer is influenced by the Asian summer monsoon. Accelerated atmospheric easterlies over the equatorial Pacific in model runs with higher mountains were associated with suppressed upwelling in the western Pacific. This increases the SWT in the western Pacific, even though the SWT decreases over most of the Pacific. In the runs with higher mountains, a thicker and warmer oceanic layer forms in the western Pacific. Therefore, the zonal gradient of ocean heat content increases along the equatorial Pacific. Thus, a La Niña-like structure of SWT along the Equator is enhanced by the increased presence of mountains. In contrast, SWT above 30 m is larger in the eastern Indian Ocean in run M than in M0, because of suppressed upwelling.

Changes in the atmospheric circulation over the tropical Pacific, which alter the tropical ocean, were also strongly related to the evolution of the Asian summer monsoon. The broad zonal SLP gradient from the eastern Pacific to the Indian Ocean increases for runs with higher mountains. Thus accelerating easterlies along the equatorial Pacific, particularly between runs M6 and M8. Diabatic heating, associated with convection over South Asia, increases in runs with higher mountains. Similarly, upper tropospheric divergence centered over South Asia strengthens in the Eastern Hemisphere. Thus, the Walker circulation between Asia, and the eastern Pacific, strengthens as mountains rise.

Precipitation centered near the dateline in the equatorial Pacific decreases as mountains rise, consistent with the cooler SSTs caused by stronger atmospheric easterlies. At the same time, precipitation increases from the maritime continent to the eastern Indian Ocean, where ascent is enhanced, as shown in Fig. 16c. The changes in the diabatic heating field, associated with convection, are consistent with a stronger Walker circulation.

Effects of large-scale orography have been investigated in the past using GCMs, but most studies did not consider ocean changes, because an AGCM was used. Thus, few studies have investigated the coupled tropical climate by including the Indian and Pacific Oceans. This study shows that large-scale orography significantly influences the formation of present features of tropical climate, both in the ocean and atmosphere. Such features are also influenced by atmosphere-ocean feedbacks, including the warm pool in the western Pacific, the Walker

Circulation and the Asian summer monsoon in the atmosphere. Thicker and warmer ocean heat content in the western Pacific, which increases in runs with higher mountains, may also affect the ENSO cycle, as suggested in Wyrtki (1975). The MRI CGCM-I was also used by Kitoh et al. (1999), who showed that simulated Indian summer monsoon rainfall anomalies were negatively correlated with equatorial Pacific SST anomalies, and by Ogasawara et al. (1999), who examined mechanisms forcing the tropospheric biennial oscillation (TBO) of the ENSO-monsoon system. Their results are consistent with the results in this study, showing that the stronger Asian summer monsoon can cool SSTs in the equatorial Pacific, by changing the east-west Walker circulation. Note that the effects of orography on interannual variability, are outside the scope of this study.

There are aspects of the coupled GCM used in this study that could be improved. The method of flux adjustment that maintains the reality of the model's surface climate in the control experiment, could affect the magnitude of the model's response. Results from climate change studies with models that do and do not include flux adjustments are broadly in agreement; however, the effect on mountain uplift studies and paleo-simulations is unknown. The need for stable models, without flux adjustments, remains an important requirement for studies that investigate the effects of mountain uplift on climate.

Acknowledgments

The authors express sincere thanks to Dr. F. Kimura, Dr. H.L. Tanaka, Dr. H. Ueda, and graduate students in the climatology and meteorology group in the University of Tsukuba for a lot of advice. We also thank two anonymous reviewers for their valuable comments. This work was done as a co-operative study between the Institute of Geoscience, University of Tsukuba and the Meteorological Research Institute. It was also partially supported by Large Scale Numerical Simulation Project of Science Information Processing Center, University of Tsukuba.

References

Abe, M., A. Kitoh and T. Yasunari, 2003: An evolution of the Asian summer monsoon associated with mountain uplift-simulation with the MRI atmosphere-ocean coupled GCM. *J. Meteor. Soc. Japan*, **81**, 909–933.

Hahn, D.G. and S. Manabe, 1975: The role of mountains in the south Asian monsoon circulation. *J. Atmos. Sci.*, **32**, 1515–1541.

Kitoh, A., 2002: Effect of large-scale mountains on surface climate—A coupled ocean-atmosphere general circulation model study—. *J. Meteor. Soc. Japan*, **80**, 1165–1181.

———, S. Yukimoto and A. Noda, 1999: ENSO-monsoon relationship in the MRI coupled GCM. *J. Meteor. Soc. Japan*, **77**, 1221–1245.

———, A. Noda, Y. Nikaidou, T. Ose and T. Tokioka, 1995: AMIP simulations of the MRI GCM. *Pap. Meteorol. Geophys.*, **45**, 121–148.

Kutzbach, J.E., W.L. Prell and W.F. Ruddiman, 1993: Sensitivity of Eurasian climate to surface uplift of the Tibetan Plateau. *J. Geology*, **101**, 177–190.

———, P.J. Guetter, W. Rudiman and W.L. Prell, 1989: Sensitivity of climate to Late Cenozoic uplift in southern Asia and the American West: numerical experiments. *J. Geophys. Res.*, **94**, 18393–18407.

Lacis, A.A. and J.E. Hansen, 1974: A parametrization for the absorption of solar radiation in the Earth's atmosphere. *J. Atmos. Sci.*, **31**, 118–133.

Liu, X. and Z.-Y. Yin, 2002: Sensitivity of East Asia monsoon climate to the uplift of the Tibetan Plateau. *Palaeogeog., Palaeoclimat., Palaeoecol.*, **183**, 223–245.

Nagai, T., T. Tokioka, M. Endoh and Y. Kitamura, 1992: El Niño-Southern Oscillation simulated in an MRI atmosphere-ocean coupled general circulation model. *J. Climate*, **5**, 1202–1233.

Ogasawara, N., A. Kitoh, T. Yasunari and A. Noda, 1999: Tropospheric biennial oscillation of ENSO-monsoon system in the MRI coupled GCM. *J. Meteor. Soc. Japan*, **77**, 1247–1270.

Palmer, T.N. and D.A. Mansfield, 1984: Response of two atmospheric general ciriculation models to sea-surface temperature anomalies in the tropical east and west Pacific. *Nature*, **310**, 483–485.

———, G.J. Shutts and R. Swinbank, 1986: Alleviation of a systematic westerly bias in general circulation and numerical weather prediction models through an orographic gravity wave drag parameterization. *Quart. J. Roy. Meteor. Soc.*, **112**, 1001–1039.

Shibata, K. and T. Aoki, 1989: An infrared radiative scheme for the numerical models of weather and climate. *J. Geophys. Res.*, **94**, 14923–14943.

Tokioka, T., K. Yamazaki, A. Kitoh and T. Ose, 1988: The equatorial 30–60 day oscillation and the Arakawa-Schubert penetrative cumulus parameterization. *J. Meteor. Soc. Japan*, **66**, 883–901.

———, A. Noda, A. Kitoh, T. Nikaidou, S. Nakagawa, T. Motoi, S. Yukimoto and K. Takata, 1995: A transient CO2 experiment with the MRI CGCM—Quick report—. *J. Meteor. Soc. Japan*, **73**, 817–826.

Wyrtki, K., 1975: El Niño—The dynamic response of the equatorial Pacific Ocean to atmospheric forcing. *J. Phys. Oceanogr.*, **5**, 572–584.

Yasunari, T., 1987: Global structure of the El Niño/Southern Oscillation Part I. El Niño Composites. *J. Meteor. Soc. Japan*, **65**, 67–80.

———, 1990: Inpact of Indian monsoon on the coupled atmopsphere/ocean system in the tropical Pacific. *Meteor. Atmos. Phys.*, **44**, 29–41.

——— and Y. Seki, 1992: Role of the Asian monsoon on the interannual variability of the gobal climate system. *J. Meteor. Soc. Japan*, **70**, 177–189.

Yukimoto, S., M. Endoh, Y. Kitamura, A. Kitoh, T. Motoi, A. Noda and T. Tokioka, 1996: Interannual and interdecadal variabilities in the Pacific in an MRI coupled GCM. *Clim. Dyn.*, **12**, 667–683.